Analysis of Human Cytochrome P450 2C8 Substrate Specificity Using a Substrate Pharmacophore and Site-Directed Mutants†

Armelle Melet,‡ Cristina Marques-Soares,‡ Guillaume A. Schoch,§ Anne-Christine Macherey,‡ Maryse Jaouen,‡ Patrick M. Dansette,‡ Marie-Agnès Sari,‡ Eric F. Johnson,§ and Daniel Mansuy*,‡

Laboratoire de Chimie et Biochimie Pharmacologiques et Toxicologiques, UMR 8601 CNRS, Université Paris 5, 45 Rue des Saints-Pères, 75270 Paris Cedex 06, France, and Department of Molecular and Experimental Medicine, The Scripps Research Institute, 10550 North Torrey Pines Road, MEM-255, La Jolla, California 92037

Received May 25, 2004; Revised Manuscript Received September 6, 2004

ABSTRACT: The structural determinants of substrate specificity of human liver cytochrome P450 2C8 (CYP2C8) were investigated using site-directed mutants chosen on the basis of a preliminary substrate pharmacophore and a three-dimensional (3D) model. Analysis of the structural features common to CYP2C8 substrates exhibiting a micromolar K_m led to a substrate pharmacophore in which the site of oxidation by CYP2C8 is 12.9, 8.6, 4.4, and 3.9 Å from features that could establish ionic or hydrogen bonds, and hydrophobic interactions with protein amino acid residues. Comparison of this pharmacophore with a 3D model of CYP2C8 constructed using the X-ray structure of CYP2C5 suggested potential CYP2C8 amino acid residues that could be involved in substrate recognition. Twenty CYP2C8 site-directed mutants were constructed and expressed in yeast to compare their catalytic activities using five CYP2C8 substrates that exhibit different structures and sizes [paclitaxel, fluvastatin, retinoic acid, a sulfaphenazole derivative (DMZ), and diclofenac]. Mutation of arginine 241 had marked effects on the hydroxylation of anionic substrates of CYP2C8 such as retinoic acid and fluvastatin. Serine 100 appears to be involved in hydrogen bonding interactions with a polar site of the CYP2C8 substrate pharmacophore, as shown by the 3−4-fold increase in the K_m of paclitaxel and DMZ hydroxylation after the S100A mutation. Residues 114, 201, and 205 are predicted to be in close contact with substrates, and their mutations lead either to favorable hydrophobic interactions or to steric clashes with substrates. For instance, the S114F mutant was unable to catalyze the 6α-hydroxylation of paclitaxel. The S114F and F205A mutants were the best catalysts for retinoic acid and paclitaxel (or fluvastatin) hydroxylation, respectively, with k_{cat}/K_m values 5 and 2.1 (or 2.4) times higher, respectively, than those found for CYP2C8. Preliminary experiments of docking of the substrate into the experimentally determined X-ray structure of substrate-free CYP2C8, which became available quite recently [Schoch, G. A., et al. (2004) *J. Biol. Chem. 279*, 9497], were consistent with key roles for S100, S114, and F205 residues in substrate binding. The results suggest that the effects of mutation of arginine 241 on anionic substrate hydroxylation could be indirect and result from alterations of the packing of helix G with helix B′.

Cytochrome P450s (CYPs)[1] constitute a superfamily of heme proteins that play important roles in the oxidative metabolism of a large variety of xenobiotics and endobiotics (*1*). The CYP2Cs make up a major subfamily of P450 enzymes that are found primarily in the liver (*2*) and, to a lesser extent, in several extrahepatic tissues (*3*−*6*). Four members of this subfamily have been identified in humans: CYP2C8, CYP2C9, CYP2C18, and CYP2C19 (*2, 7*). Although the sequences of the four isoforms are more than 80% identical, they have distinct substrate specificities. Understanding the structural basis of these substrate specificities has been the objective of many laboratories.

CYP2C9 and CYP2C19 have been the most studied human CYP2C isoforms because of their important roles in drug metabolism and drug interactions. Their active sites and binding determinants were initially characterized using biochemical, UV−visible, and ^{1}HNMR spectroscopy (*8*−*14*), three-dimensional (3D) molecular models (*8*, *10*, *14*−*24*), and site-directed mutants (*18*, *22*, *25*−*30*) as reviewed in refs *31* and *32*. Recently, the X-ray structures of substrate-free CYP2C9 and of the CYP2C9−warfarin (*33*) and CYP2C9−flurbiprofen (*34*) complexes have been reported.

By comparison, little was known about the active site of CYP2C8. Fewer CYP2C8 substrates are currently listed in the Human Metabolism Database (http://www.gentest.com/human_p450_database) compared to the number listed for CYP2C9 and CYP2C19. Moreover, most of these CYP2C8 substrates have been proposed on the basis of experiments

† The research was supported by funds from CNRS and Ministry of Research (France) (group of D.M.) and by the U.S. National Institutes of Health (Grant GM031001, group of E.F.J.).

* To whom correspondence should be addressed. Telephone: 33 1 42 86 21 69. Fax: 33 1 42 86 83 87. E-mail: daniel.mansuy@univ-paris5.fr.

‡ UMR 8601 CNRS.

§ The Scripps Research Institute.

[1] Abbreviations: CH_3COOH, acetic acid; CH_3CN, acetonitrile; CYP, cytochrome P450; DMSO, dimethyl sulfoxide; DMZ, 4-methyl-*N*-methyl-*N*-(2-phenyl-2*H*-pyrazol-3-yl)benzene sulfonamide; GRID/CPCA, GRID program/Consensus Principal Component Analysis; 3D, three-dimensional; SRS, substrate recognition site; SD, standard deviation.

10.1021/bi0489309 CCC: $27.50
Published on Web 11/18/2004

performed with human liver microsomes using correlation or inhibition studies. The kinetic parameters of purified CYP2C8 for these substrates have been rarely determined. In fact, few high-affinity substrates have been identified so far, and most were characterized recently. This is the case for drugs exhibiting very different structures such as paclitaxel (*35*), fluvastatin (*36*), troglitazone (*37*), amiodarone (*38*), amodiaquine (*39*), or tazarotenic acid (*40*). These recently identified substrates suggest that the role of CYP2C8 in drug metabolism has been underestimated. CYP2C8 also catalyzes the oxidation of endogenous compounds such as retinoids (*41*, *42*) and arachidonic acid (*43*, *44*). Some metabolites of arachidonic acid act as endothelium-derived hyperpolarizing factors (EDHFs) with vasodilator properties (*45*), and several studies suggest that CYP2C8 could be a possible EDHF synthase involved in the regulation of vascular homeostasis (*46*−*48*).

Homology models (*23*, *39*, *49*), based on the first X-ray structure published for a mammalian cytochrome P450, rabbit CYP2C5 (*50*), have been reported recently for CYP2C8. The first model of CYP2C8 was published in 2001 by Ridderstrom et al. in combination with a GRID/CPCA selectivity analysis of human CYP2C models (*23*). This selectivity analysis singled out CYP2C8 as the most distinct of the four human CYP2C enzymes because of big differences in the size and properties of some putative active site amino acids such as residues 114, 205, and 476. Docking of some substrates such as rosiglitazone (*49*) and amodiaquine (*39*) into CYP2C8 models has led the authors to propose substrate interactions with residues Asn99, Ser114, and Phe205.

Although homology models have been published for CYP2C8, no substrate pharmacophore has been proposed to date and no study based on site-directed mutants has been reported.[2] This work was performed in an effort to investigate the structural determinants of CYP2C8 substrate specificity. It involved the following steps: (a) the construction of a pharmacophore of the CYP2C8 substrates and of a 3D model of CYP2C8, (b) the choice of 20 site-directed mutations on the basis of possible interactions between CYP2C8 substrates (pharmacophore) and the CYP2C8 model, and (c) a comparison of the catalytic properties of the corresponding mutants toward five CYP2C8 substrates exhibiting different structures. As these studies were being completed, the X-ray structure of substrate-free CYP2C8 at a resolution of 2.7 Å became available (*51*), which allowed preliminary docking experiments for verifying interactions with some of the substrates that were experimentally analyzed with the site-directed mutants.

EXPERIMENTAL PROCEDURES

Materials

Oligonucleotides were synthesized by Genome Express (Paris, France) or Eurogenentec (Seraing, Belgium). The TG1 *Escherichia coli* strain [*D(lac pro) supE thi hsdD5 F′ traD35 proAB LacIq LacZDM15*] was used for plasmid amplification. *Saccharomyces cerevisiae* strains W(N) and W(R) and the yeast expression vector pYeDP60 were a gift from D. Pompon (CNRS, Gif-sur-Yvette, France). W303-1B (MAT **a**; *ade2*-1; *his3*-11,-15; *leu2*-3,-112; *ura3*-1; *trp1*-1) designated as W(N) was described previously (*52*). Yeast strain W(R) was constructed from strain W(N) by substitution of the natural promoter of the W303-1B gene encoding cytochrome P450 reductase with the galactose-inducible *GAL10-CYC1* hybrid promoter (*53*). The CYP2C8 expression vector was constructed by insertion of the CYP2C8 cDNA into the pYeDP60 polylinker as reported previously (*54*). Growth media for *E. coli* and *S. cerevisiae* were obtained from Difco (Coger, France) or GibcoBRL (Cergy-Pontoise, France). Restriction endonucleases and DNA modification enzymes were of the best available grade. Plasmid DNA was isolated with the plasmid miniprep kit from Bio-Rad (Marnes la Coquette, France). NADPH, NADP, glucose 6-phosphate, and glucose-6-phosphate dehydrogenase were purchased from Roche Diagnostics (Meylan, France). Fluvastatin was provided by Merck Lipha, and diclofenac, retinoic acid, and sulfaphenazole were provided by Sigma (St. Quentin Fallaviers, France). Troglitazone was purchased from Cayman Chemicals (SPI-BIO, Massy, France). 4-Methyl-*N*-methyl-*N*-(2-phenyl-2*H*-pyrazol-3-yl)benzene sulfonamide (DMZ) was synthesized according to previously described procedures (*55*). All other materials not listed were obtained from standard sources.

Site-Directed Mutagenesis

Site-directed mutagenesis of CYP2C8 was performed by two successive PCRs followed by homologous recombination in yeast (*56*, *57*). The general procedures and PCR conditions were described previously (*29*). The mutagenic primers are listed in Table 1. The final PCR product was cotransformed into yeast strain W(N) with double-digested *Bam*HI−*Eco*RI plasmid expression vector pYeDP60. The DNA of the gap repair clones was extracted according to a method described previously (*58*) and electroporated into TG1 *E. coli*. For all the selected plasmids, the entire coding region was sequenced by Genome Express (Grenoble, France) to confirm the incorporation of the desired mutation without extraneous changes.

Yeast Transformation, Cell Culture, and Preparation of the Yeast Microsomal Fraction

The expression system used for human liver P450s was based on yeast strain W(R) previously described (*53*), in which yeast cytochrome P450 reductase was overexpressed. Yeast transformation by the pYeDP60 vector containing *CYP*2C8 or mutated cDNAs was performed as described previously (*53*, *58*). Yeast culture and microsome preparation are described elsewhere (*59*). Microsomes were homogenized in 50 mM Tris buffer (pH 7.4) containing 1 mM EDTA and 20% glycerol (v/v), aliquoted, frozen under liquid N_2, and stored at −80 °C until they were used. The microsomal P450 content was determined according to the method of Omura and Sato (*60*). The NADPH-cytochrome P450 reductase activity was measured spectroscopically by the method of Vermilion and Coon (*61*) by monitoring the reduction of cytochrome *c* at 550 nm (ϵ_{550} = 21 400 M^{-1} cm^{-1}). The protein content in microsomal suspensions was measured by the Bradford procedure (*62*) using bovine serum albumin as the standard.

[2] During the revision of the manuscript, data about CYP2C8 mutants at positions 113, 114, 359, 362, and 366 have been reported (*77*).

Table 1: Oligonucleotides Used in the Construction of CYP2C8 Mutants[a]

mutation	primer sequence
R97A	5′-TGGGGAATTGCCT**GC**TCCAGAAAACTC-3′
R97K	5′-TGGGGAATTGCC**TTT**TCCAGAAAACTC-3′
N99L	5′-GATATTGGGGAA**AG**GCCTCTTCCAG-3′
S100A	5′-TGAGATATTGG**GG**CATTGCCTCTTCCAG-3′
S103A	5′-GTAATTCTTTGA**GC**TATTGGGGAATTG-3′
R105A	5′-CAAGTCCTTTAGTAATT**GC**TTGAGATATTGGGGAATTGC-3′
S114A	5′-CTTTCCATTGCTGG**C**AATGATTCCAAGTC-3′
S114F	5′-TCCATTGCTG**A**AAATGATTCCAAGTCC-3′
F201L	5′-CTGAGTTTTCATT**C**AATCTTTTCATC-3′
F205A	5′-CATGGGGAGTTCAGAATCCTG**GC**GTTTTCATTGAATC-3′
F205I	5′-CTGGATCCACGGGGAGTTCAGAATCCTGA**T**GTTTTCATTGAATC-3′
R241A	5′-CTAATGTAACTT**GC**TGTAAGAGCA-3′
R241L	5′-GTTGCTCTTACA**CT**AAGTTACATTAGGGAG-3′
R241E	5′-GTTGCTCTTACA**GA**AAGTTACATTAGGGAG-3′
S359I	5′-CAGAGATACA**TT**GACCTCGTCCCCAC-3′
A471P	5′-GAACCTCAATACTACT**C**CAGTTACCAAAG-3′
T473V	5′-CTACTGCAGTT**GT**CAAAGGGATTGTTTC-3′
K474N	5′-CTGCAGTTACCAA**T**GGGATTGTTTC-3′
I476F	5′-GTTACCAAAGGGTT**T**TGTTTCTCTG-3′
S482F	5′-CTCTGCCACCCT**TC**TACCAGATCTGCTTC-3′

[a] Changed nucleotides are in bold. Codons for the changed amino acids are underlined. Primers from mutations R97A to R241A are reverse oligonucleotides.

Immunoblotting

Electrophoresis was carried out using a Bio-Rad Mini Protean II device. Proteins were separated on a 10% SDS−PAGE gel (*63*) and transferred to a nitrocellulose membrane using a Transblot semi-dry transfer cell from Bio-Rad. The membrane was blocked and probed as previously described (*64*) with a rabbit polyclonal anti-P450 2C antibody kindly provided by P. Beaune (Inserm U490, Paris, France).

Molecular Modeling

Molecular modeling was performed with the Insight II software package from Molecular Simulations Inc. (San Diego, CA).

Pharmacophore Modeling. Five known substrates of CYP2C8 with K_m values of ≤ 10 μM were compared. The initial geometries of four substrates (paclitaxel, retinoic acid, troglitazone, and amiodarone) were taken from the Cambridge Structural Database. The conformation of fluvastatin was calculated using four InsightII modules (Builder, Discover_3, Ampac-Mopac, and Biopolymer_3). The molecule was first built using the Builder program and energy minimized using the Discover_3 module, using the method of steepest descent followed by conjugate gradient minimization with the esff force field. Partial atom charges were then calculated (Ampac-Mopac module) and used in a final energy minimization of the fluvastatin 3D structure (Biopolymer_3 module). The most rigid substrates, retinoic acid and fluvastatin, were first superimposed with respect to their oxidation sites, using the Transform-Superimpose module of Insight II. Then all the other molecules were successively overlayed by the same method. The final superimposition highlighted several common structural features.

CYP2C8 3D Model. A 3D model of CYP2C8 was constructed by virtual mutagenesis of rabbit CYP2C5 (*50*), according to previously described procedures (*29*, *65*). Fluvastatin was placed in the distal binding pocket, in an orientation consistent with the experimentally observed product. The structure was minimized using the Docking module of Insight II.

Docking of Substrates into the Experimentally Determined Structure of CYP2C8. Computer-assisted automated docking of substrates into the experimentally determined structure of CYP2C8 employed Autodock 3.05, a grid-based docking program (*66*). Autodock uses a search method based on a modified genetic algorithm that employs a local search in identifying low-energy binding sites and orientations of the probe molecule. For each docking run, a $58 \times 74 \times 60$ grid with a spacing of 0.375 Å was used that encompassed the active site of the A model of the 1PQ2 structure. Explicit polar hydrogens were included in the model. Kollman united atom charges were assigned to the protein using Autodocktools. Charges for the heme were assigned as described by Helms and Wade (*67*). Charges were assigned to retinoic acid, fluvastatin, and paclitaxel using the Prodrg (*68*) server (http://davapc1.bioch.dundee.ac.uk/programs/prodrg/). The results of 50 randomly seeded runs were examined to identify solutions that placed the substrate in the active site at positions appropriate for hydroxylation.

Enzyme Activity Assays

General Enzyme Assay Conditions. Incubations for metabolic activity with yeast microsomes were carried out at 28 °C, using glass tubes in a shaking bath. The incubation mixtures contained yeast microsomes (0.05 μM P450), the substrate, and a NADPH-generating system (1 mM $NADP^+$, 10 mM glucose 6-phosphate, and 2 units of glucose-6-phosphate dehydrogenase per milliliter) diluted in a 50 mM Tris buffer (pH 7.4) containing 1 mM EDTA and 8% glycerol (final concentrations). Activity assays were routinely initiated ($t_0 = 0$ min) by addition of the NADPH-generating system to the incubation mixture after a 3 min preincubation at 28 °C for temperature equilibration. Several incubation times were used, generally 1, 2, and 3 min. These times were increased, up to 6 times, in the case of low-activity mutants. At t_0 and regularly thereafter, aliquots (100−120 μL) were taken and the reaction was quickly stopped by treatment with 0.5 volume of a cold CH_3CN/CH_3COOH (10:1) mixture containing 5 μM internal standard (final concentration). Proteins were then sedimented by centrifugation for 5 min

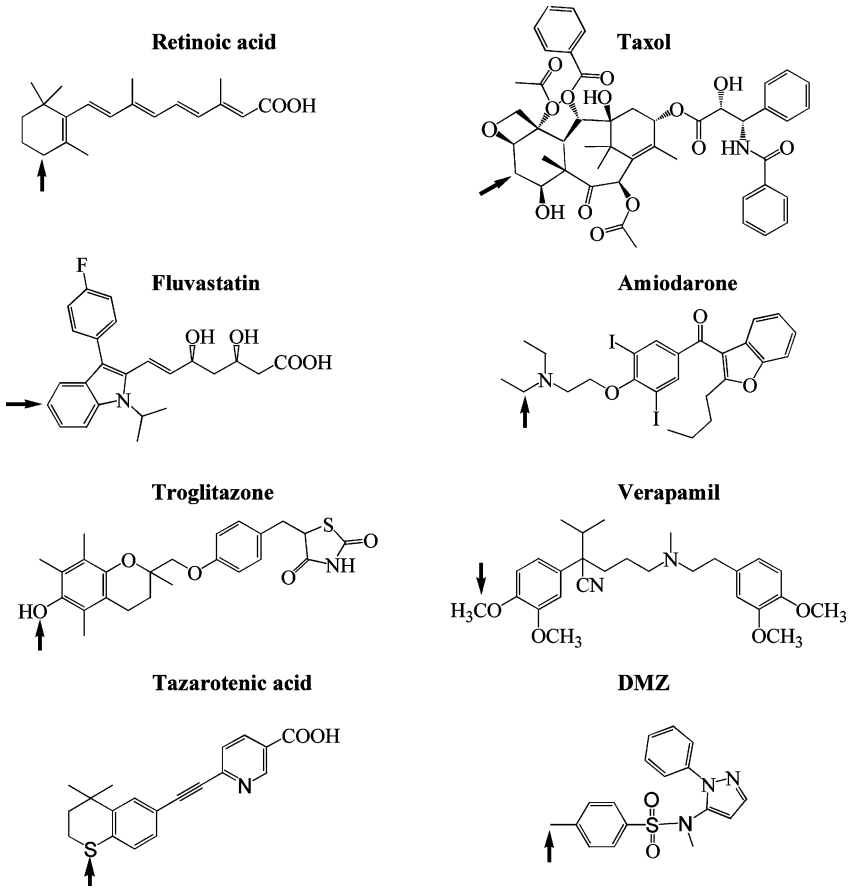

FIGURE 1: Structures of CYP2C8 substrates mentioned in the text. Arrows indicate the major site of oxidation by CYP2C8. Molecules on the left side are anionic at physiological pH; molecules on the right side are neutral or cationic.

at 10 000 rpm, and the supernatant was analyzed by reverse phase HPLC at 40 °C (Spectra system AS 3000 autosampler).

In experiments with retinoic acid, reactions were stopped with 1 volume of a cold CH_3CN/CH_3COOH (10:1) mixture containing 5 μM internal standard and 1 mg/mL butylated hydroxytoluene as an antioxidant. All the procedures were carried out under darkness or subdued lighting.

Paclitaxel 6α-Hydroxylation. 6α-Hydroxylation of paclitaxel by CYP2C8 (*35*) and its mutants was performed under the conditions described above, with tienilic acid as the internal standard. Samples were injected onto a X-Terra MS C18 column (Waters) (250 mm × 4.6 mm, 5 μm). The mobile phase (A, 5 mM H_3PO_4; B, CH_3CN) was delivered at a rate of 1 mL/min with the following gradient: linear gradient from 30 to 45% B for 5 min, a second linear gradient to 55% B over the course of 25 min, a third linear gradient to 100% B over the course of 1 min, and hold for 5 min. Inhibition studies were performed at various concentrations of inhibitors (1−100 μM) and at the K_m concentration of paclitaxel for CYP2C8 or its mutants. The inhibitor and the substrate dissolved in DMSO (final concentration of 1%) were added simultaneously to the incubation mixture.

Fluvastatin 5-Hydroxylation. This hydroxylation (*36*) was performed under the conditions described above, with cerivastatin as the internal standard. Samples were injected onto a C8 Hypersil MOS column (Thermohypersil-Keystone) (250 mm × 4.6 mm, 5 μm). The mobile phase [A, 0.1 M ammonium acetate (pH 4.6); B, $CH_3CN/MeOH/H_2O$ (7:2:1)] was delivered at a rate of 1 mL/min with the following gradient: 17% B for 2 min followed by a linear gradient to 100% B over the course of 25 min followed by an additional 5 min elution. The 5-hydroxyfluvastatin metabolite was quantitated using UV detection at 250 nm.

Retinoic Acid 4-Hydroxylation. This hydroxylation (*42*) was performed under the conditions described above, with tienilic acid as the internal standard. Samples were injected onto a C8 Hypersil MOS column (Thermohypersil-Keystone) (250 mm × 4.6 mm, 5 μm). The mobile phase [A, 0.1 M ammonium acetate (pH 4.6); B, $CH_3CN/MeOH/H_2O$ (7:2:1)] was delivered at a rate of 1 mL/min with the following gradient: 17% B for 2 min, a linear gradient to 100% B over the course of 20 min, and hold for 15 min.

Diclofenac Hydroxylation. Diclofenac hydroxylation was monitored at 280 nm according to a previously described procedure (*29*).

DMZ Hydroxylation. The incubation conditions are described above. HPLC procedures for the analysis of DMZ hydroxylation were derived from a previously described protocol (*55*). Samples were injected onto a C8 Hypersil MOS column (Thermohypersil-Keystone) (250 mm × 4.6 mm, 5 μm). The mobile phase [A, H_2O; B, $CH_3CN/MeOH/H_2O$ (7:2:1)] was pumped at a rate of 1 mL/min according to the following gradient: 100% A for 1 min followed by a linear gradient to 100% B over the course of 23 min and hold for 6 min. Monitoring of the column effluent was performed at 230 nm.

RESULTS AND DISCUSSION

Structural Comparison of High-Affinity CYP2C8 Substrates and Construction of a Preliminary Substrate Phar-

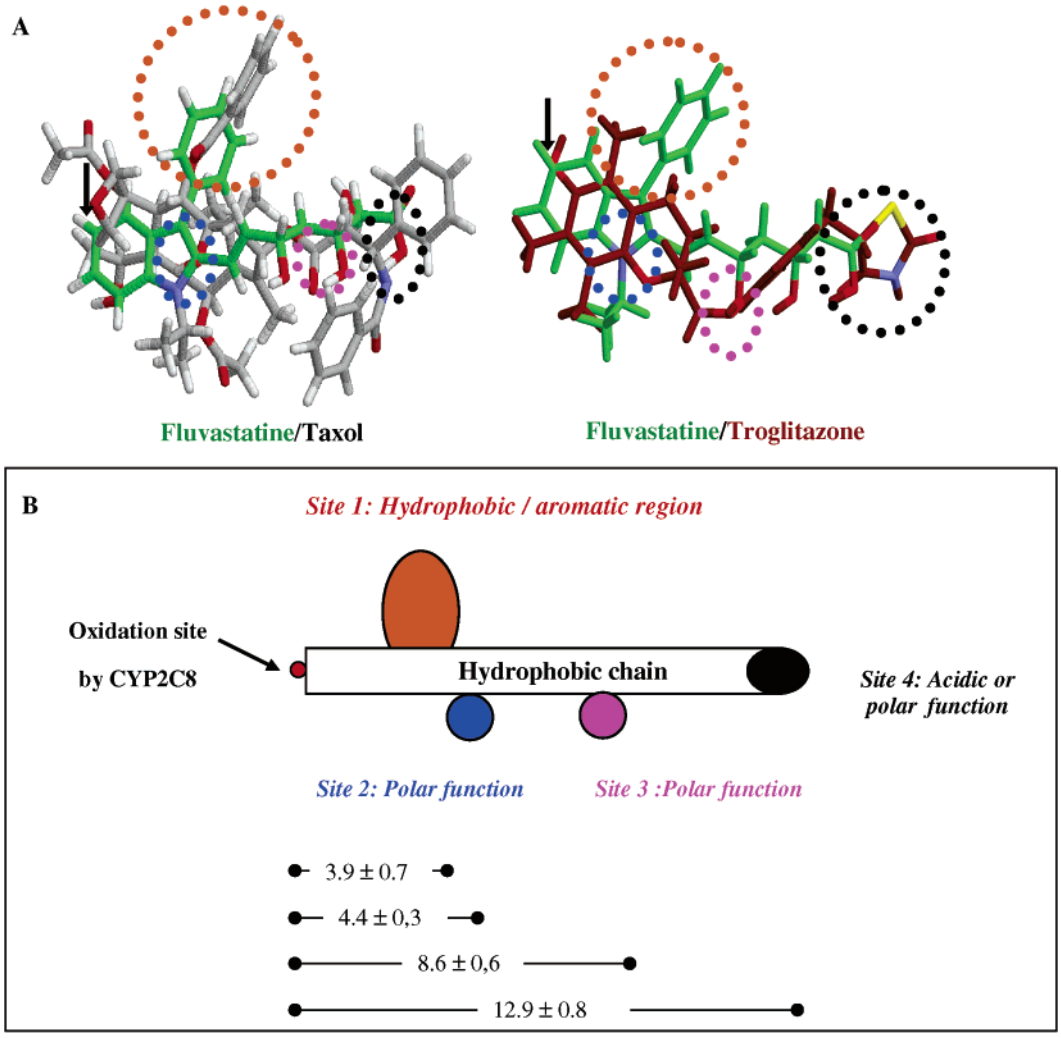

FIGURE 2: Pharmacophore model of CYP2C8 substrates. (A) Examples of superimpositions of substrates performed to constuct the pharmacophore (fluvastatin and paclitaxel, and fluvastatin and troglitazone). Sites of oxidation by CYP2C8 are denoted with arrows. Common structural features of the substrates that correspond to sites 1−4 of the pharmacophore (Figure 2B) are circled using colors identical to those of the corresponding pharmacophore sites. (B) Pharmacophore model of CYP2C8 substrates. Sites 1−4 indicate common structural features that could represent sites of interaction with CYP2C8. Site 1 could provide π-stacking or hydrophobic interactions. Sites 2 and 3 are potential hydrogen-bonding sites. Site 4 could form ionic or hydrogen bonds with CYP2C8 residues. Distances were measured in angstroms between the oxidized atom and the anchoring carbon of site 1 on the main chain of the substrate, and between the oxidized atom and the heteroatom possibly involved in hydrogen or ionic bonds of sites 2−4.

macophore. Substrates of CYP2C8 displaying a micromolar K_m and reported to be mainly oxidized at only one position were used to find common structural determinants and to build a preliminary substrate pharmacophore. Five molecules, paclitaxel (*35*), retinoic acid (*42*, *69*), fluvastatin (*36*), troglitazone (*37*), and amiodarone (*38*), fulfilled the criteria. Figure 1 shows that these compounds exhibit very different structures and indicates the main oxidation site by CYP2C8.

The major conformations of these substrates either were obtained from their corresponding X-ray structure or were deduced from molecular modeling calculations (see Experimental Procedures). The pharmacophore was built by superimposition of the substrates on two template molecules, retinoic acid and fluvastatin, by matching their oxidation sites in the first step and then by looking for analogous functional groups.

Analysis of the overlay (Figure 2A) indicates common structural characteristics of these substrates. As shown in Figures 1 and 2, all of the compounds have a long hydrophobic chain with an acidic (pK < 7) or polar group 12.9 ± 0.8 Å from the oxidation site (site 4 in Figure 2B) and a hydrophobic or aromatic moiety 3.9 ± 0.7 Å from the oxidation site (site 1 in Figure 2B). Retinoic acid, fluvastatin, and troglitazone are negatively charged at physiological pH, and their terminal polar groups are carboxylate functions for the two former molecules or a $(CO)_2N^-$ function from the thiazolidinedione ring of the latter. In paclitaxel and amiodarone, site 4 is a neutral, polar group, i.e., the oxygen atom of the amide function of paclitaxel and the oxygen atom of the benzofurane ring of amiodarone. Two supplementary polar groups (sites 2 and 3 in Figure 2B) are also present in all of the substrates except retinoic acid. They are located 4.4 ± 0.3 and 8.6 ± 0.3 Å from the oxidation site. They are a hydroxyl and an ester keto group in paclitaxel, a nitrogen atom and a hydroxyl group in fluvastatin, a heterocyclic oxygen atom and another ether oxygen atom in troglitazone, and an iodine atom and the oxygen atom of the keto function in amiodarone.

Two medium-affinity substrates of CYP2C8, the drug verapamil (K_m = 50−185 μM) (*70*, *71*) and a recently

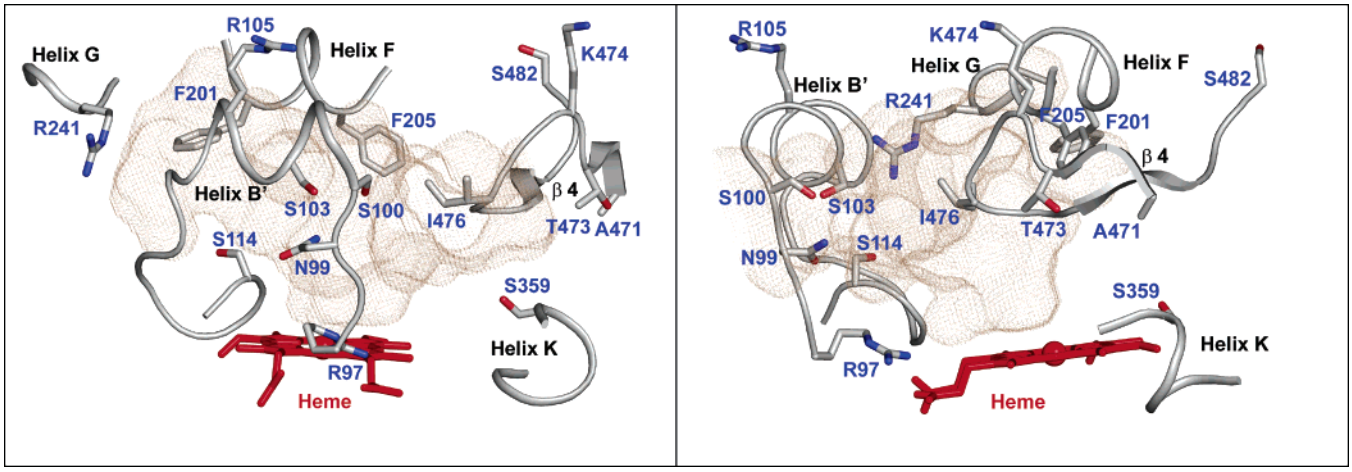

FIGURE 3: Orthogonal views of the substrate binding cavity of CYP2C8 (PDB entry 1PQ2) depicting residues selected for mutagenesis in this study. Residues mutated in this study are depicted as stick figures and identified by blue labels. The surface (in gray) of the substrate binding cavity is rendered as mesh, and was calculated using a 1.4 Å probe with VOIDOO (*76*). This figure was generated using PYMOL (http://www.pymol.org).

described substrate of CYP2C5 and human CYP2Cs, DMZ (see Figure 1 for its formula; $K_m = 40 \pm 5$ μM) (*55*), were then overlaid on the pharmacophore. Verapamil fit with the model even though it was somewhat longer than the other substrates. Sites 4, 3, and 2 correspond to the oxygen of an OCH_3 substituent, the tertiary amine nitrogen atom, and the cyano function of verapamil, respectively. DMZ is much smaller than the other substrates and was overlaid with the portion of the pharmacophore that is close to the oxidation site (sites 2 and 1 corresponding to the SO_2 and phenyl groups of DMZ, respectively). This poorer fit of verapamil and DMZ to the pharmacophore could explain their lower affinity for CYP2C8. Finally, a recently described substrate of CYP2C8, tazarotenic acid (Figure 1) (*40*) ($K_i \approx 30$ μM), could easily be incorporated into the pharmacophore as its carboxylate function and pyridine nitrogen atom corresponded to sites 4 and 3, respectively.

Construction of a 3D Model of CYP2C8 and Choice of the Mutants. A tentative 3D model of CYP2C8 was constructed by virtual mutagenesis of CYP2C5 using the X-ray structure of CYP2C5 (*50*), and procedures identical to those previously reported for constructing 3D models of CYP2C9 (*29*) and of CYP2Bs (*65*). The main structural characteristics of the active site of our model were very similar to those of other previously reported CYP2C8 models (*23*, *39*, *49*). The CYP2C8 active site appeared to be much larger than those of other CYP2Cs even though it is somewhat height-limited by Phe205, which is specific for CYP2C8 and located in the roof of the active site. This was in agreement with a previously reported CYP2C8 model (*23*) and was confirmed by an X-ray structure of substrate-free CYP2C8 (*51*) that became available at the end of the work described in this article.

Docking of substrates such as fluvastatin in the active site of the CYP2C8 model suggested some amino acid residues from the protein that could interact with the different structural features of the substrate pharmacophore model. For instance, in our preliminary CYP2C8−fluvastatin model, the carboxylate and fluorophenyl groups of the substrate interacted with the Arg241 guanidinium group and the Phe205 phenyl group, respectively. Moreover, Asn99 and Ser114 from the B−C loop were not far from the substrate, and given the flexibility of this loop upon substrate binding to P450 2Cs (*72*, *73*), these residues could be involved in hydrogen bonding interactions with the hydroxyl groups of fluvastatin.

Such a preliminary analysis led us to select Arg241 and two other arginines of the B−C loop, Arg105 and Arg97, as possible candidates for interactions with the negatively charged or polar terminal groups of CYP2C8 substrates (site 4 of the pharmacophore). These arginines were first mutated to alanines (R97A, R105A, and R241A). Arg97 and 241 were later substituted with other residues (R97K, R241L, and R241E) to improve the understanding of the importance of these two amino acid positions.

On the basis of the same analysis, Phe205, and another aromatic residue, Phe201, from substrate recognition site 2 (SRS2) of CYP2 proteins according to Gotoh (*74*), were selected as candidates for hydrophobic interactions with the hydrophobic region of substrates (site 1 of the pharmacophore). Phe201 and Phe205 were mutated to Leu or Ile, to suppress the aromatic ring with minimal changes in side chain hydrophobicity and bulk (F201L and F205I). The F205A mutant was also constructed to investigate the influence of the side chain length at this position.

As far as residues possibly establishing hydrogen bonds with sites 2 and 3 of the pharmacophore (Figure 2B) are concerned, not only Asn99 and Ser114 but also serines 100, 103, and 359, which are polar residues specific to CYP2C8 within the human CYP2C family, were selected for site-directed mutagenesis. Serine residues 100, 103, and 114 were replaced with alanines (S100A, S103A, and S114A), and Asn99 was replaced with a leucine (N99L) to suppress the polar function with minimal change in the side chain bulk. Ser114 was also replaced with a bulky phenylalanine, which is present in other CYP2Cs such as CYP2C9, CYP2C18, CYP2C19, and CYP2C5.

In our CYP2C8−fluvastatin model, Ile476 was sufficiently close to the central phenyl group of fluvastatin to form hydrophobic contacts. Although this residue did not interact with an identified pharmacophore motif of fluvastatin, we decided to further investigate the role of Ile476 and other

residues of the C-terminal loop (Ala471, Thr473, Lys474, and Ser482) that are specific to CYP2C8 within the human CYP2C subfamily. These amino acids were mutated to the corresponding residues in CYP2C9.

All the aforementioned residues (except Arg241 and Ser482) are predicted to reside in substrate recognition sites SRS1, SRS2, SRS5, and SRS6 of CYP2 proteins according to Gotoh (*74*). Figure 3 shows the positioning of the mutated residues in the X-ray structure of free CYP2C8 (*51*), which became available before completion of this work. It appears that most of the mutated residues are either within or in the proximity of the CYP2C8 active site.

Construction and Expression of CYP2C8 Mutants. All of the CYP2C8 mutants were constructed using a double-PCR approach followed by homologous recombination in yeast (*56*, *57*). The mutants were expressed in yeast strain W(R) that overexpresses cytochrome P450 reductase (*53*). Immunoblotting using anti-CYP2C IgG revealed the immunoreactive protein in all microsomal preparations (data not shown). In their Fe(II) state, all the mutants bound CO as evidenced by the appearance of a 450 nm peak in visible difference spectroscopy. Only small peaks at 420 nm corresponding to <10% cytochrome P420 were observed. Recombinant P450 specific contents in yeast microsome preparations were calculated from the difference spectra and were 60 ± 30 pmol of CYP/mg of microsomal protein for CYP2C8 and varied from 13 to 77 pmol of CYP/mg of protein for the various mutants. The yeast P450 reductase: CYP molar ratio was 2 ± 0.5 for wild-type CYP2C8 and ranged from 1.5 to 2.7 for the mutants, except for S114F, S359I, and S482F, for which it was larger (4 ± 0.5). The data indicate that there was sufficient reductase in the preparations of yeast microsomes containing each mutant for P450 monoxygenase activities.

Catalytic Activities of CYP2C8 Mutants. Initial characterization of the catalytic activities of CYP2C8 and its mutants was performed on three different CYP2C8 substrates (paclitaxel, retinoic acid, and fluvastatin) at a single concentration much higher than the reported K_m of the wild-type enzyme (Figure 4). The oxidation of these substrates at the positions indicated in Figure 1 was followed by HPLC (see Experimental Procedures). The paclitaxel hydroxylation rates were not significantly different from those of wild-type CYP2C8, except for the R97A, R97K, S114F, and F205I mutants, and to a lesser extent for R105A. R97K and F205I displayed 10-fold lower activity than CYP2C8. The extent of hydroxylation of paclitaxel was drastically reduced in the case of R97A (1% of CYP2C8 activity) and was not even detectable with the S114F mutant (even after an extended 30 min incubation). In contrast, the R105A mutant exhibited slightly increased activity.

The retinoic acid hydroxylation rates were similar to those of the wild-type enzyme except for the R97A, R97K, R105A, S114A, F201L, I476F, and S482F mutants. The R97A, R97K, F201L, and I476F mutants were 8, 4, 2, and 2 times less active than CYP2C8, respectively, whereas R105A, S114A, and S482F were slightly more active.

A greater number of mutants displayed altered catalytic activities toward fluvastatin. Fluvastatin hydroxylation rates were not significantly changed by the S103A, R105A, S359I, A471P, and S482F mutations, while all the other mutants exhibited activity significantly lower or higher than that of

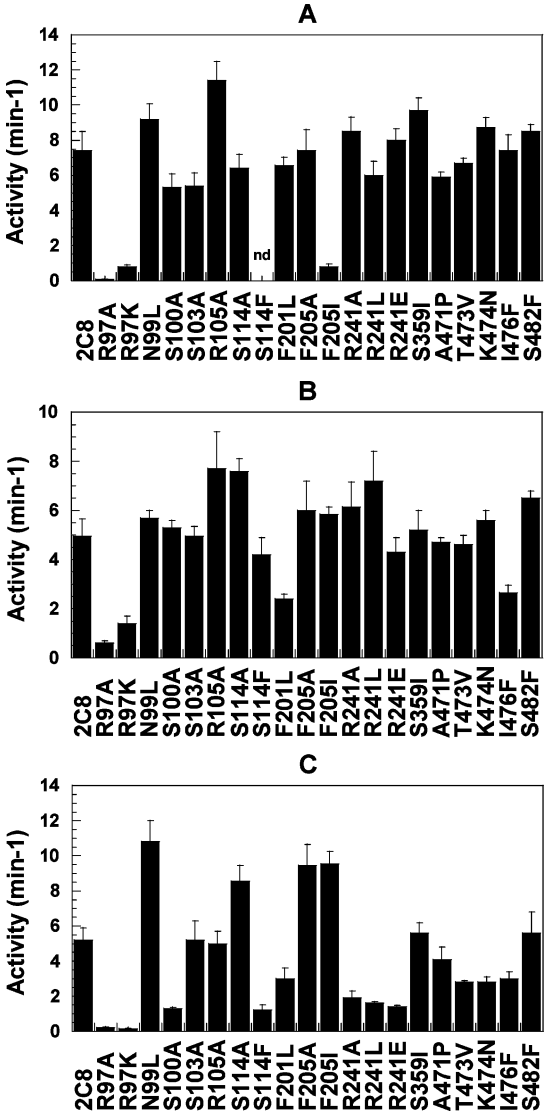

FIGURE 4: Hydroxylase activities of yeast-expressed CYP2C8 and its mutants at a single substrate concentration: (A) 50 μM paclitaxel, (B) 200 μM retinoic acid, and (C) 100 μM fluvastatin. Assays were performed as described in Experimental Procedures. Mean values ± the standard deviation from three experiments.

CYP2C8. The most spectacular effects were again observed with the R97A and R97K mutants which exhibited ~3% of the wild-type activity. The S100A and S114F mutations led to a 4-fold decrease in the fluvastatin hydroxylation rate, and the R241A, R241L, and R241E mutations caused a 3-fold decrease in activity. The F201L, T473V, K474N, and I476F mutants exhibited a lower activity than CYP2C8, whereas the N99L, F205A, and F205I mutants exhibited a 2-fold increase in activity.

According to these results, mutations at positions 97 (SRS1), 114 (SRS1), and 205 (SRS2) produced the most notable effects, by significantly altering the hydroxylation rates of at least two tested substrates. Substitutions of Arg97 with alanine or lysine caused a spectacular decrease in the hydroxylation rates of all the tested substrates. In contrast, mutations at position 114 and 205 led to a behavior that was dependent on the substrate and nature of the substituted amino acids.

A more detailed study of the effects of the mutations on the recognition and hydroxylation of substrates by CYP2C8

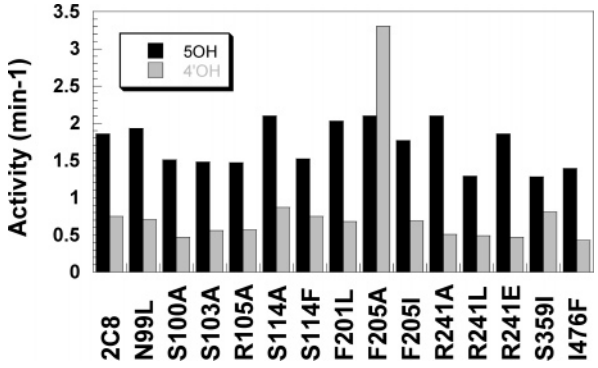

FIGURE 5: Regioselectivity of diclofenac hydroxylation by yeast-expressed CYP2C8 and several mutants. 4′- and 5-hydroxylation activities (min^{-1}) were measured at 800 μM diclofenac, as described in Experimental Procedures. Listed values are the mean of two experiments. The variablity between each of the duplicate values was $\leq$10%.

was performed to determine the kinetic constants of the oxidation of four substrates, retinoic acid, fluvastatin, paclitaxel, and DMZ. The different structural characteristics of these substrates allowed us to probe different aspects of CYP2C8 binding and catalysis. For instance, retinoic acid and fluvastatin are anionic molecules at physiological pH (with a carboxylate function as site 4), whereas paclitaxel and DMZ are neutral. DMZ, the shortest molecule, does not contain any functional group at site 4 in the pharmacophore. Paclitaxel and fluvastatin involve two matching polar functions (sites 2 and 3 of the pharmacophore, Figure 2B); on the other hand, DMZ only bears the polar group at site 2, and retinoic acid has no groups at these sites. The CYP2C8 mutants were also compared for their regioselectivity of diclofenac hydroxylation (Figure 5), as CYP2C8 produces both 5-hydroxy- and 4′-hydroxydiclofenac, whereas CYP2C9 is highly regioselective, with the almost exclusive formation of 4′-hydroxydiclofenac (*75*).

The detailed kinetic studies were performed with most of the mutants. Recent reports indicate that Arg97 is involved in heme binding by CYP2C5 and CYP2C9 proteins, as clearly shown in the X-ray structures of the CYP2C5−DMZ (*72*) and CYP2C5−diclofenac (*73*) complexes, and of CYP2C9 (*33*). The dramatic decrease in the activities of CYP2C8 upon mutation of Arg97, which was observed with all the tested substrates (Figure 4), may reflect major changes in the active site resulting from modifications in heme binding. Very similar results have been obtained after mutation of Arg97 in CYP2C9 (*28*). Therefore, mutants R97A and R97K were not studied in more detail, as altered kinetic characteristics may not be strictly related to the mode of substrate binding by CYP2C8.

The results obtained with the other mutants are presented by groups of mutated residues that could interact with the different sites on the pharmacophore model (Figure 2B).

Effects of Mutations of Arginines 105 and 241. Tables 2 and 3 show that the R105A mutation has only very small effects on CYP2C8 catalytic efficiency (k_{cat}/K_m) with all of the substrates studied. Only small increases in the K_m values were observed for fluvastatin and paclitaxel hydroxylation. Similar results indicating that Arg105 does not play an important role in substrate binding have been published for the CYP2C9 R105A mutant (*28*). Interestingly, mutation of Arg241 led to different effects as a function of the substrate

Table 2: Kinetic Parameters for Retinoic Acid 4-Hydroxylation and Fluvastatin 5-Hydroxylation by Yeast-Expressed CYP2C8 and Its Mutants[a]

	retinoic acid 4-hydroxylation			fluvastatin 5-hydroxylation		
CYP	K_m (μM)	k_{cat} (min^{-1})	k_{cat}/K_m[b]	K_m (μM)	k_{cat} (min^{-1})	k_{cat}/K_m[b]
2C8	32 ± 4	6 ± 1	0.2	29 ± 4	7 ± 2	0.25
R105A	33 ± 4	9 ± 2	0.3	56 ± 6	8 ± 1.5	0.14
R241A	66 ± 7	7.6 ± 1	0.1	113 ± 11	4 ± 0.7	0.03
R241L	57 ± 5	9 ± 1	0.2	102 ± 14	2.2 ± 0.6	0.02
R241E	61 ± 4	5 ± 1	0.08	126 ± 11	2.2 ± 0.4	0.02
F201L	17 ± 2	2.6 ± 0.5	0.15	29 ± 3	3 ± 0.5	0.1
F205A	119 ± 13	9 ± 2	0.08	29 ± 2	18 ± 3	0.6
F205I	17 ± 2	7 ± 1	0.4	38 ± 5	18 ± 4	0.5
N99L	30 ± 3	7 ± 1	0.2	25 ± 4	13 ± 1	0.5
S100A	28 ± 6	6 ± 1	0.2	38 ± 7	1.3 ± 0.2	0.03
S103A	45 ± 6	6 ± 1	0.13	37 ± 4	9 ± 2	0.2
S114A	52 ± 11	11 ± 2	0.2	29 ± 5	13 ± 1	0.4
S114F	4 ± 1	4.5 ± 1	1.1	40 ± 6	1.7 ± 0.3	0.04
S359I	44 ± 3	6.6 ± 1	0.15	38 ± 6	7 ± 1	0.2
I476F	26 ± 6	3 ± 0.4	0.1	58 ± 7	4.5 ± 0.6	0.08

[a] K_m and k_{cat} were estimated by nonlinear regression analysis of the rate vs concentration; assays were performed as described in Experimental Procedures. Mean values ± SD from three experiments. [b] k_{cat}/K_m in min^{-1} μM^{-1}.

Table 3: Kinetic Parameters for Paclitaxel 6α-Hydroxylation and DMZ Hydroxylation by Yeast-Expressed CYP2C8 and Its Mutants[a]

	paclitaxel 6α-hydroxylation			DMZ 4-hydroxylation		
CYP	K_m (μM)	k_{cat} (min^{-1})	k_{cat}/K_m[b]	K_m (μM)	k_{cat} (min^{-1})	k_{cat}/K_m[b]
2C8	10 ± 2	9 ± 2	0.9	37 ± 4	16 ± 6	0.4
R105A	19 ± 3	16 ± 2	0.8	49 ± 7	24 ± 4	0.5
R241A	15 ± 1	11 ± 1	0.7	94 ± 14	19 ± 4	0.2
R241L	13 ± 1	8 ± 1	0.6	37 ± 6	52 ± 6	1.4
R241E	13 ± 1	10 ± 2	0.8	43 ± 2	13 ± 1	0.3
F201L	24 ± 5	9.7 ± 0.3	0.4	79 ± 9	16 ± 3	0.2
F205A	4 ± 1	8 ± 1	2	158 ± 30	56 ± 10	0.35
F205I	14 ± 1	0.9 ± 0.1	0.06	73 ± 5	26 ± 4	0.35
N99L	23 ± 1	13 ± 2	0.6	32 ± 3	38 ± 5	1.2
S100A	44 ± 5	9 ± 1	0.2	123 ± 10	11 ± 1	0.09
S103A	14 ± 1	7 ± 1	0.5	26 ± 3	32 ± 5	1.2
S114A	9 ± 2	8 ± 1	0.9	18 ± 5	20 ± 3	1.1
S114F	−	<0.1[c]	−	38 ± 8	45 ± 7	1.2
S359I	8 ± 1	10 ± 2	1.2	nd[d]	nd[d]	nd[d]
I476F	15 ± 1	10 ± 1	0.7	nd[d]	nd[d]	nd[d]

[a] K_m and k_{cat} were estimated by nonlinear regression analysis of the rate vs concentration. Assays were performed as described in Experimental Procedures. Mean values ± SD from three experiments. [b] k_{cat}/K_m in min^{-1} μM^{-1}. [c] Formation of 6α-hydroxypaclitaxel was not detected under our conditions. [d] Not determined.

structure. The K_m values for the hydroxylation of neutral substrates such as paclitaxel and DMZ did not significantly change upon mutation of Arg241 (except for the particular case of DMZ and R241A). By contrast, the K_m values determined for the hydroxylation of the acidic substrates, retinoic acid and fluvastatin, which contain a carboxylate group at pharmacophore site 4 (at physiological pH), increased in the R241 mutants (2- and 4-fold increases for retinoic acid and fluvastatin, respectively). This was accompanied by a marked decrease in the catalytic efficiency for fluvastatin hydroxylation (k_{cat}/K_m 10-fold lower). These results suggest that Arg241 could be involved in an interaction with the terminal function of substrates (site 4 in Figure 2B). This binding interaction should be stronger with

Table 4: Comparison of K_m or IC_{50} of CYP2C8 and Its R241A Mutant toward Four Substrates[a]

substrate (site 4 at physiological pH)	K_m or IC_{50} (μM)	
	2C8	R241A
paclitaxel (CONH)	10 ± 1	15 ± 1
retinoic acid (COO^-)	32 ± 2	86 ± 5
fluvastatin (COO^-)	29 ± 2	113 ± 11
troglitazone ($CO-N^--CO$)	*8 ± 1*	*48 ± 7*

[a] K_m values are derived from Tables 2 and 3. IC_{50} (in italics) are the concentrations of troglitazone that inhibit 50% of 6α-hydroxylation of paclitaxel (10 or 15 μM, K_m values) by CYP2C8 and its R241A mutant. Assay conditions are described in Experimental Procedures. Mean values ± SD from three experiments.

substrates bearing a negative charge at site 4 that could establish an ionic bond with the guanidinium group of Arg241. To confirm this assumption, experiments were carried out with CYP2C8 and the R241A mutant to compare the inhibitory effects of another CYP2C8 substrate bearing a terminal anionic function at site 4, troglitazone (Figure 1). Table 4 shows that troglitazone is a better inhibitor of CYP2C8 than of the R241A mutant (IC_{50} values of 8 ± 1 and 48 ± 7 μM, respectively). The data listed in Table 4 indicate that substrates bearing a terminal negative charge (retinoic acid, fluvastatin, and troglitazone) have a higher affinity for CYP2C8 than for the R241A mutant (3−6-fold increase in K_m or IC_{50}), whereas a neutral substrate, paclitaxel, exhibits similar affinities for CYP2C8 and the R241A mutant. The equivalent of Arg241 in CYP2C5, Lys241, is located at the entrance of the substrate access channel of CYP2C5 (*50*). Moreover, in the X-ray structure of the CYP2C5−diclofenac complex (*73*), the terminal carboxylate group of diclofenac is engaged in the substrate access channel and is separated from Lys241 by a network of water molecules.

The small effects of the R241L and R241E mutations on the K_m of hydroxylation of DMZ, a neutral substrate that is too short to interact with Arg241, are in agreement with the above-mentioned role of Arg241. The increased K_m found for DMZ hydroxylation after the R241A mutation, and not after the R241L or R241E mutation, could reflect the short length of DMZ and more favorable interactions in the slightly smaller active sites of CYP2C8 and the R241E and R241L mutants when compared to the R241A mutant. Interestingly, the R241L mutant was the most efficient catalyst of DMZ hydroxylation, as it showed a k_{cat}/K_m value of 1.4 min^{-1} μM^{-1}, which is more than 3 times greater than that of CYP2C8. This increase in catalytic efficiency is only due to an increase in k_{cat} (Table 3).

Effects of Mutations of Phenylalanines 201 and 205. Mutations of Phe201 and -205 affected CYP2C8 kinetic parameters in a substrate-dependent manner. They had very small effects on the K_m of fluvastatin hydroxylation, whereas they had large and differing effects on the K_m of hydroxylation of the three other substrates. The loss of the phenyl ring of Phe201 or -205 in the F201L, F205A, and F205I mutants increased the K_m of DMZ hydroxylation, and the effect was larger in the F205A mutant (4-fold instead of 2-fold). This could be related to the loss of favorable $\pi-\pi$ interactions between these protein phenyl rings and the phenyl ring of DMZ (site 1 in Figure 2B). The much larger K_m increase displayed by the F205A mutant probably reflects less favorable hydrophobic interactions between the DMZ phenyl ring and the methyl group of F205A, when compared with the alkyl groups of F201L and F205I.

Mutations of Phe201 and Phe205 had differing effects on the observed K_m for retinoic acid and paclitaxel hydroxylation. Mutations F201L and F205I led to a 2-fold decrease in the K_m of retinoic acid hydroxylation, whereas mutation F205A produced a 4-fold increase. In contrast, mutations F201L and F205I produced a small increase in the K_m of paclitaxel hydroxylation, whereas mutation F205A elicited a 2-fold decrease. These effects may reflect the very different structures and sizes of these two substrates. The loss of $\pi-\pi$ interactions between a phenyl ring of paclitaxel (site 1) and the phenyl rings of Phe201 and 205 could explain the increase in the K_m of paclitaxel hydroxylation observed with the F201L and F205I mutations. In the case of retinoic acid, stronger hydrophobic interactions between hydrophobic site 1 of the pharmacophore (corresponding to the dimethyl-substituted part of the cyclohexyl group) with the alkyl chain of Leu201 or Ile205 than with the phenyl group of Phe201 (or Phe205) would explain the decrease in K_m, observed with the F201L and F205I mutations.

If Phe205 is in contact with substrates in the CYP2C8 active site, then the F205A mutation would provide more space above the heme, leading to a better accommodation of paclitaxel, the biggest substrate that has been studied. The additional space would also account for the weaker binding of retinoic acid as it would allow more mobility and reduced position restraints in the active site. In that regard, it is noteworthy that mutation F205A is the only one that gave a significant increase in the catalytic efficiency of CYP2C8 for paclitaxel hydroxylation (2-fold increase in k_{cat}/K_m, Table 3). Moreover, the F205A mutation produced the most spectacular change in the regioselectivity of diclofenac hydroxylation, as it was the only mutation that produced an inversion of the 5-hydroxydiclofenac:4′-hydroxydiclofenac ratio in favor of 4′-hydroxylation (Figure 5). Taken together, these data indicate that amino acid 205 is an important determinant in substrate positioning in the CYP2C8 active site.

Effects of Mutations of Asn99, Ser100, Ser103, Ser114, and Ser359. The S103A, S359I, and N99L mutations produced relatively minor effects on the catalytic properties of CYP2C8 toward the four studied substrates. However, there was a significant increase in the K_m of paclitaxel hydroxylation (2-fold increase) and also an increase in the k_{cat} for the hydroxylation of three substrates observed with the N99L mutant.

In contrast, the results shown in Tables 2 and 3 suggest that Ser100 could be involved in hydrogen bonding interactions with site 2 of the substrate pharmacophore (Figure 2B). Indeed, the S100A mutation displayed an increased K_m for hydroxylation of paclitaxel and DMZ (between 3- and 5-fold, Table 3), two CYP2C8 substrates involving features at site 2 in the pharmacophore that can easily establish a hydrogen bond with Ser100 (a hydroxyl and a SO_2 function, respectively, Figure 1). In contrast, the K_m for hydroxylation of retinoic acid, which has no polar group at pharmacophore site 2 (Figure 1) and should not bind to Ser100, was not significantly changed in the S100A mutant (Table 2). In fact, the kinetic constants of retinoic acid hydroxylation were not affected by this mutation. Finally, the catalytic efficiency of

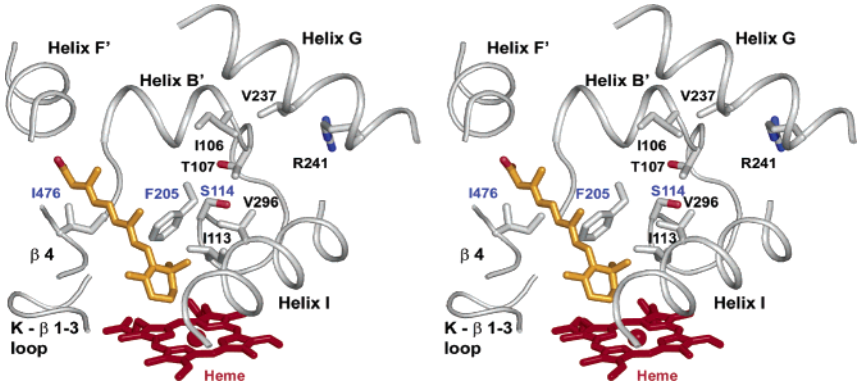

FIGURE 6: Computational docking of retinoic acid in the experimentally determined structure of CYP2C8 (PDB entry 1PQ2). Residues mutated in this study that altered retinoic acid hydroxylation are labeled in blue together with docked retinoic acid (in yellow). The S114F change produces a 7-fold decrease in K_m. Basic residues are not available within the active site for interaction with the carboxylate. The side chains of residues 106, 107, 113, 114, 237, and 296 prevent direct interactions between the side chain of retinoic acid and the guanidine group of R241. This figure was generated using PYMOL.

mutant S100A for fluvastatin hydroxylation was considerably lower (8-fold) than that of CYP2C8.

The hydroxyl of Ser114 seems to be much less important for substrate recognition than that of Ser100, because the S114A mutation did not affect the K_m values of paclitaxel and fluvastatin hydroxylations, only slightly increased the K_m of retinoic acid hydroxylation, and even decreased by a factor 2 the K_m of DMZ hydroxylation. However, residue 114 appears to be in the proximity of the substrates in the CYP2C8 active site, as it has been shown to be in CYP2C9 by a mutagenesis study (*29*), because the S114F mutation led to dramatic and contrasting effects on CYP2C8 substrate hydroxylation. The S114F mutant was completly inactive for paclitaxel hydroxylation, and this may reflect space constraints on the very bulky paclitaxel substrate imposed by increasing the size of residue 114. On the other hand, the S114F mutant exhibited a much better affinity for retinoic acid, with an 8-fold lower K_m value (Table 2), than CYP2C8. This may reflect the long hydrophobic chain of this substrate, which is not too bulky (when compared to paclitaxel). The space constraints and possible supplementary interactions supplied by the phenyl group of Phe114 from mutant S114F could promote optimal binding. Interestingly, the S114F mutant exhibited the highest catalytic efficiency for retinoic acid hydroxylation, and its k_{cat}/K_m value was 5-fold higher than that of CYP2C8.

Effects of the I476F Mutation. Mutation I476F in CYP2C8 had small effects on the hydroxylation of retinoic acid and paclitaxel. However, it led to a 2-fold increase in the K_m of fluvastatin hydroxylation and a 3-fold decrease in the k_{cat}/K_m of this reaction (Tables 2 and 3).

Automated Docking Studies Using the Experimentally Determined Structure of CYP2C8. Quite recently, the structure of CYP2C8 was determined to 2.7 Å by X-ray diffraction (*51*). The structure of CYP2C8 in the absence of a substrate exhibits a closed structure with an active site volume that is 2-fold larger than that seen for the structure of CYP2C5 used to model CYP2C8. The larger active site of 2C8 extends outward from the heme between β-sheet 1 and helix F′, and the overall shape and polarity of the active site cavity differ from those seen in CYP2C5 (*50*, *72*, *73*). Preliminary substrate docking experiments using this experimentally determined structure were carried out in an effort to further understand the results obtained with the site-directed mutants. The computer-simulated docking studies were carried out using Autodock (*66*). The program permits rotations around bonds in the substrate when it searches for a fit. However, the protein model is static. Comparisons of structures determined for different substrate complexes with CYP2C5 indicate that some regions of the active site, particularly helix B′ and helices F and G, are relatively flexible and move to accommodate substrates of different sizes (*72*, *73*). Thus, conformational changes in the protein induced by substrate binding could lead to solutions that are not predicted from the static model of the substrate-free protein. In this regard, docking of paclitaxel in the active site proved to be relatively difficult as slight differences produce highly unfavorable scores. Although a reasonable docking location was found (not shown), the tight fit suggests that the structure is likely to change with paclitaxel bound.

Retinoic acid is a long molecule that is relatively rigid due to the conjugation of the double bonds in the hydrophobic side chain bearing the carboxylate group. For the docking, rotations were permitted for the carboxylate moiety and the ring relative to the side chain. Autodock predicts a single docking location in the active site with the site of hydroxylation located close to the heme iron (Figure 6). The carboxylate is oriented toward the entrance of the solvent channel that occurs on the N-terminal side of helix B′ rather than on the C-terminal side as in CYP2C5. The strongest effects of mutagenesis on retinoic acid oxidation were obtained with the F205A mutant that exhibited a 4-fold decrease in binding affinity and with the S114F mutant that displayed a 7-fold increase in binding affinity. Mutations in helix B′ had little effect on the oxidation of retinoic acid. This is consistent with the docking of this substrate (Figure 6) in a position that does not contact the mutated residues in helix B′ and that allows room for S114F mutation. The decrease in the apparent K_m seen for the S114F mutant would be consistent with a reduction in the degree of motion of retinoic acid in the binding site cavity effected by the presence of the larger side chain, whereas the F205A mutation may have the opposite effect.

In contrast to the restricted docking results with retinoic acid, a relatively large number of reasonable locations and orientations were predicted for fluvastatin binding reflecting the size of the active site cavity and the flexibility of the substrate. Only those predictions that placed the site of

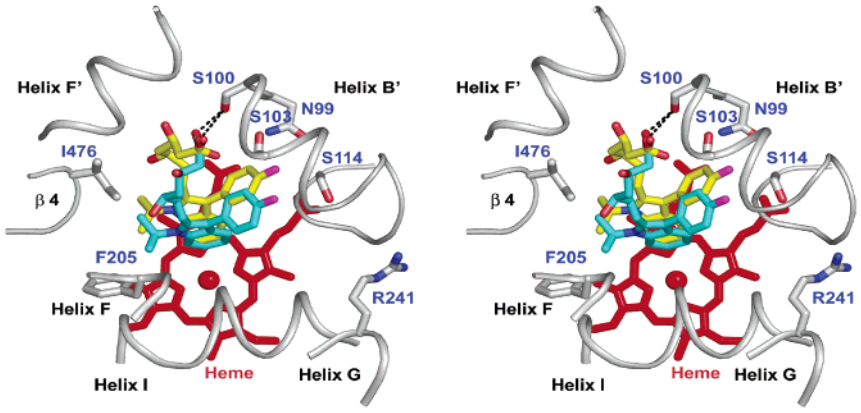

FIGURE 7: Alternate predictions for the docking of fluvastatin. Two docking solutions for fluvastatin (yellow and blue) illustrate the potential to accommodate the polar side chain of the substrate in alternative conformations that maintain a productive orientation for metabolism in the proximity of the heme (red) iron. There is a close correspondence of the two molecules near the heme iron, whereas the flexible alkyl-carboxylic side chains exhibit different conformations. In both cases, the substrate interacts with S100 of helix B′. Side chains of mutated residues that affect fluvastatin 5-hydroxylation are labeled in blue. This figure was generated using PYMOL.

hydroxylation in a reasonable position for oxidation are considered here. As depicted in Figure 7, the polar side chain of fluvastatin can adopt more than one orientation that is both reasonable and consistent with the observed regiospecificity of hydroxylation. The carboxylate of fluvastatin interacts with polar residues in the first turn of helix B′ (Figure 7) through potential hydrogen bonding interactions. Consistent with the docking result, the S100A mutation decreases k_{cat}/K_m for fluvastatin 5-hydroxylation by 8-fold. In contrast, the S100A mutation has no effect on retinoic acid hydroxylation, consistent with a lack of apparent hydrogen bonding interactions between retinoic acid and this region. The effects of mutations N99L, S114F, F205A/I, and I476F on fluvastatin oxidation are consistent with the docking results as these residues are all close to the docked substrate (Table 2 and Figure 7).

The differential effects of mutating R241 on the oxidation of retinoic acid and fluvastatin are also consistent with the docking results. The docking prediction for retinoic acid places the carboxylate moiety far from R241 (Figure 6), and relatively small effects of the R241 mutations are observed on its hydroxylation relative to what would be expected for hydrogen bonding stabilized by the attraction of complementary charges. However, the R241 mutations have a greater effect on fluvastatin hydroxylation. The carboxylate side chains of all of the substrates are prevented from interacting directly with the guanidine group of R241 by steric hindrance created by several residues depicted in Figure 7. The effect of R241 mutations on fluvastatin binding may result from alterations of the packing of helix G with helix B′ that result from mutation of residue 241. The C-terminal end of helix B′ interacts directly with R241 and adjacent residues. Noticeably, the charge inversion in the R241E mutant does not significantly increase the effect when compared to the R241L and R241A mutations, which is consistent with the absence of a required role in providing a stabilizing ionic interaction with the substrate within the interior of the active site cavity. Alternatively, relatively small conformation changes in helix B′, such as those seen in CYP2C5 upon binding of different substrates (*72*, *73*), could increase the accessibility of R241 to the substrates leading to the potential for more direct interactions.

CONCLUSION

The very recent X-ray structure of substrate-free CYP2C8 (*51*) indicates that CYP2C8 has an especially large active site when compared with other CYP2C structures. This great size should permit more substrate mobility and more possible interactions with the protein residues. It also explains the great diversity of CYP2C8 substrate structures and the ability to accommodate large substrates such as paclitaxel (Figure 1). However, this renders more difficult any general substrate pharmacophore determination and any explanation of the effects of site-directed mutations on substrate binding and hydroxylation. In that context, our studies provide initial data on a limited number of known high-affinity (micromolar K_m) substrates that will help to clarify the presumably complex problem of substrate recognition by CYP2C8.

Our analysis of the structural determinants that are common to eight CYP2C8 substrates, and of the protein residues that could be involved in the binding of the corresponding functional groups present in the pharmacophore (on the basis of the study of 20 site-directed mutants), leads to the following propositions.

(1) Most of the studied substrates involve a terminal anionic or polar function ~13 Å from the hydroxylation site, and one or two secondary polar functions ~8.5 and ~4.5 Å from the site of hydroxylation. The relatively extended polar region of the helix B′ and surrounding regions of the protein may contribute to an increased number of high-affinity binding conformations by offering the substrate multiple binding modes that are favorable for hydrogen bonding. The increased entropy due to multiple conformations of the bound substrate may contribute significantly to a favorable free energy for binding of flexible substrates such as fluvastatin. These polar interactions are also consistent with the pharmacophore model, which emphasizes the polarity of the CYP2C8 substrates distal from the site of hydroxylation. Ser100 is a residue in helix B′ that appears to play an important role in substrate binding (see Tables 2 and 3 and Figure 7). Asn99 could also be involved in the binding of paclitaxel (Table 3). Mutation of Arg 241 has important effects on the kinetics of CYP2C8-mediated hydroxylation of anionic substrates. However, the molecular origin of these effects remains to be established.

(2) Residues 201, 205, and 114 appear to be in close contact with the substrates. As a function of the nature and size of these residues in CYP2C8 or its mutants, and of the substrate structure, these residues may establish either favorable π-stacking (CYP2C8 and paclitaxel and DMZ) or hydrophobic (F201L or F205I and retinoic acid, S114F and retinoic acid) interactions, or unfavorable steric interactions (S114F and paclitaxel).

In relation with these important roles of Phe205 and Ser114, it is noteworthy that significant improvements of the catalytic efficiencies of CYP2C8 have been obtained by mutating these residues. Thus, among all the mutants described above, S114F was the most efficient catalyst for retinoic acid hydroxylation, with a k_{cat}/K_m value 5 times higher than that of CYP2C8. Also, F205A was the best catalyst for paclitaxel and fluvastatin hydroxylation with k_{cat}/K_m values 2.1 and 2.4 times higher, respectively, than those of CYP2C8.

A more detailed understanding of the diverse modes of substrate binding in the active site of CYP2C8 and of the effects of mutations, particularly the R241 mutations, will be obtained after the crystal structures of several CYP2C8−substrate complexes have been determined.

ACKNOWLEDGMENT

We thank Dr. Roger Attias (UMR 8601) for his help in the molecular modeling experiments on CYP2C8 and its substrates.

REFERENCES

1. Ortiz de Montellano, P. R. (1995) *Cytochrome P450: structure, mechanism and biochemistry*, Plenum Press, New York.
2. Guengerich, F. P. (1995) in *Cytochrome P450: Structure, Mechanism, and Biochemistry* (Ortiz de Montellano, P. R., Ed.) pp 473−535, Plenum Press, New York.
3. Zeldin, D. C., DuBois, R. N., Falck, J. R., and Capdevila, J. H. (1995) Molecular cloning, expression and characterization of an endogenous human cytochrome P450 arachidonic acid epoxygenase isoform, *Arch. Biochem. Biophys. 322*, 76−86.
4. Lin, H. C. J., Kobari, Y., Zhu, Y., Stemerman, M. B., and Pritchard, K. A. J. (1996) Human umbilical vein endothelial cells express P450 2C8 mRNA: Cloning of endothelial P450 epoxygenase, *Endothelium 4*, 219−229.
5. Klose, T. S., Blaisdell, J. A., and Goldstein, J. A. (1999) Gene structure of CYP2C8 and extrahepatic distribution of the human CYP2Cs, *J. Biochem. Mol. Toxicol. 13*, 289−295.
6. Ding, X., and Kaminsky, L. S. (2003) Human extrahepatic cytochromes P450: Function in xenobiotic metabolism and tissue-selective chemical toxicity in the respiratory and gastrointestinal tracts, *Annu. Rev. Pharmacol. Toxicol. 43*, 149−173.
7. Goldstein, J. A., and de Morais, S. M. (1994) Biochemistry and molecular biology of the human CYP2C subfamily, *Pharmacogenetics 4*, 285−299.
8. Mancy, A., Broto, P., Dijols, S., Dansette, P. M., and Mansuy, D. (1995) The substrate binding site of human liver cytochrome P450 2C9: An approach using designed tienilic acid derivatives and molecular modeling, *Biochemistry 34*, 10365−10375.
9. Mancy, A., Dijols, S., Poli, S., Guengerich, P., and Mansuy, D. (1996) Interaction of sulfaphenazole derivatives with human liver cytochromes P450 2C: Molecular origin of the specific inhibitory effects of sulfaphenazole on CYP 2C9 and consequences for the substrate binding site topology of CYP 2C9, *Biochemistry 35*, 16205−16212.
10. He, M., Korzekwa, K. R., Jones, J. P., Rettie, A. E., and Trager, W. F. (1999) Structural forms of phenprocoumon and warfarin that are metabolized at the active site of CYP2C9, *Arch. Biochem. Biophys. 372*, 16−28.
11. Ha-Duong, N. T., Dijols, S., Marques-Soares, C., Minoletti, C., Dansette, P. M., and Mansuy, D. (2001) Synthesis of sulfaphenazole derivatives and their use as inhibitors and tools for comparing the active sites of human liver cytochromes P450 of the 2C subfamily, *J. Med. Chem. 44*, 3622−3631.
12. Ha-Duong, N. T., Marques-Soares, C., Dijols, S., Sari, M. A., Dansette, P. M., and Mansuy, D. (2001) Interaction of new sulfaphenazole derivatives with human liver cytochrome p450 2Cs: Structural determinants required for selective recognition by CYP 2C9 and for inhibition of human CYP 2Cs, *Arch. Biochem. Biophys. 394*, 189−200.
13. Ha-Duong, N. T., Dijols, S., Macherey, A. C., Goldstein, J. A., Dansette, P. M., and Mansuy, D. (2001) Ticlopidine as a selective mechanism-based inhibitor of human cytochrome P450 2C19, *Biochemistry 40*, 12112−12122.
14. Poli-Scaife, S., Attias, R., Dansette, P. M., and Mansuy, D. (1997) The substrate binding site of human liver cytochrome P450 2C9: An NMR study, *Biochemistry 36*, 12672−12682.
15. Smith, D. A., and Jones, B. C. (1992) Speculations on the substrate structure−activity relationship (SSAR) of cytochrome P450 enzymes, *Biochem. Pharmacol. 44*, 2089−2098.
16. Jones, B. C., Hawksworth, G., Horne, V. A., Newlands, A., Morsman, J., Tute, M. S., and Smith, D. A. (1996) Putative active site template model for cytochrome P4502C9 (tolbutamide hydroxylase), *Drug Metab. Dispos. 24*, 260−266.
17. Lewis, D. F. (1998) The CYP2 family: Models, mutants and interactions, *Xenobiotica 28*, 617−661.
18. Jung, F., Griffin, K. J., Song, W., Richardson, T. H., Yang, M., and Johnson, E. F. (1998) Identification of amino acid substitutions that confer a high affinity for sulfaphenazole binding and a high catalytic efficiency for warfarin metabolism to P450 2C19, *Biochemistry 37*, 16270−16279.
19. Payne, V. A., Chang, Y. T., and Loew, G. H. (1999) Homology modeling and substrate binding study of human CYP2C18 and CYP2C19 enzymes, *Proteins 37*, 204−217.
20. Ekins, S., Bravi, G., Binkley, S., Gillespie, J. S., Ring, B. J., Wikel, J. H., and Wrighton, S. A. (2000) Three- and four-dimensional-quantitative structure activity relationship (3D/4D-QSAR) analyses of CYP2C9 inhibitors, *Drug Metab. Dispos. 28*, 994−1002.
21. Afzelius, L., Zamora, I., Ridderstrom, M., Andersson, T. B., Karlen, A., and Masimirembwa, C. M. (2001) Competitive CYP2C9 inhibitors: Enzyme inhibition studies, protein homology modeling, and three-dimensional quantitative structure−activity relationship analysis, *Mol. Pharmacol. 59*, 909−919.
22. Tsao, C. C., Wester, M. R., Ghanayem, B., Coulter, S. J., Chanas, B., Johnson, E. F., and Goldstein, J. A. (2001) Identification of human CYP2C19 residues that confer S-mephenytoin 4′-hydroxylation activity to CYP2C9, *Biochemistry 40*, 1937−1944.
23. Ridderstrom, M., Zamora, I., Fjellstrom, O., and Andersson, T. B. (2001) Analysis of selective regions in the active sites of human cytochromes P450, 2C8, 2C9, 2C18, and 2C19 homology models using GRID/CPCA, *J. Med. Chem. 44*, 4072−4081.
24. De Groot, M. J., Alex, A. A., and Jones, B. C. (2002) Development of a combined protein and pharmacophore model for cytochrome P450 2C9, *J. Med. Chem. 45*, 1983−1993.
25. Ibeanu, G. C., Ghanayem, B. I., Linko, P., Li, L. P., Pedersen, L. G., and Goldstein, J. A. (1996) Identification of residues 99, 220, and 221 of human cytochrome P450 2C19 as key determinants of omeprazole hydroxylase activity, *J. Biol. Chem. 271*, 12496−12501.
26. Klose, T. S., Ibeanu, G. C., Ghanayem, B. I., Pedersen, L. G., Li, L., Hall, S. D., and Goldstein, J. A. (1998) Identification of residues 286 and 289 as critical for conferring substrate specificity of human CYP2C9 for diclofenac and ibuprofen, *Arch. Biochem. Biophys. 357*, 240−248.
27. Haining, R. L., Jones, J. P., Henne, K. R., Fisher, M. B., Koop, D. R., Trager, W. F., and Rettie, A. E. (1999) Enzymatic determinants of the substrate specificity of CYP2C9: Role of B′−C loop residues in providing the π-stacking anchor site for warfarin binding, *Biochemistry 38*, 3285−3292.
28. Ridderstrom, M., Masimirembwa, C., Trump-Kallmeyer, S., Ahlefelt, M., Otter, C., and Andersson, T. B. (2000) Arginines 97 and 108 in CYP2C9 are important determinants of the catalytic function, *Biochem. Biophys. Res. Commun. 270*, 983−987.
29. Melet, A., Assrir, N., Jean, P., Pilar Lopez-Garcia, M., Marques-Soares, C., Jaouen, M., Dansette, P. M., Sari, M. A., and Mansuy, D. (2003) Substrate selectivity of human cytochrome P450 2C9: Importance of residues 476, 365, and 114 in recognition of diclofenac and sulfaphenazole and in mechanism-based inactivation by tienilic acid, *Arch. Biochem. Biophys. 409*, 80−91.
30. Flanagan, J. U., McLaughlin, L. A., Paine, M. J., Sutcliffe, M. J., Roberts, G. C., and Wolf, C. R. (2003) Role of conserved Asp293

of cytochrome P450 2C9 in substrate recognition and catalytic activity, *Biochem. J. 370*, 921−926.
31. Domanski, T. L., and Halpert, J. R. (2001) Analysis of mammalian cytochrome P450 structure and function by site-directed mutagenesis, *Curr. Drug Metab. 2*, 117−137.
32. Lewis, D. F. (2003) Essential requirements for substrate binding affinity and selectivity toward human CYP2 family enzymes, *Arch. Biochem. Biophys. 409*, 32−44.
33. Williams, P. A., Cosme, J., Ward, A., Angove, H. C., Matak Vinkovic, D., and Jhoti, H. (2003) Crystal structure of human cytochrome P450 2C9 with bound warfarin, *Nature 424*, 464−468.
34. Wester, M. R., Yano, J. K., Schoch, G. A., Yang, C., Griffin, K. J., Stout, C. D., and Johnson, E. F. (2004) The structure of human cytochrome P450 2C9 complexed with flurbiprofen at 2.0 Å resolution, *J. Biol. Chem. 279*, 35630−35637.
35. Rahman, A., Korzekwa, K. R., Grogan, J., Gonzalez, F. J., and Harris, J. W. (1994) Selective biotransformation of taxol to 6α-hydroxytaxol by human cytochrome P450 2C8, *Cancer Res. 54*, 5543−5546.
36. Fischer, V., Johanson, L., Heitz, F., Tullman, R., Graham, E., Baldeck, J. P., and Robinson, W. T. (1999) The 3-hydroxy-3-methylglutaryl coenzyme A reductase inhibitor fluvastatin: Effect on human cytochrome P-450 and implications for metabolic drug interactions, *Drug Metab. Dispos. 27*, 410−416.
37. Yamazaki, H., Shibata, A., Suzuki, M., Nakajima, M., Shimada, N., Guengerich, F. P., and Yokoi, T. (1999) Oxidation of troglitazone to a quinone-type metabolite catalyzed by cytochrome P-450 2C8 and P-450 3A4 in human liver microsomes, *Drug Metab. Dispos. 27*, 1260−1266.
38. Ohyama, K., Nakajima, M., Nakamura, S., Shimada, N., Yamazaki, H., and Yokoi, T. (2000) A significant role of human cytochrome P450 2C8 in amiodarone N-deethylation: An approach to predict the contribution with relative activity factor, *Drug Metab. Dispos. 28*, 1303−1310.
39. Li, X. Q., Bjorkman, A., Andersson, T. B., Ridderstrom, M., and Masimirembwa, C. M. (2002) Amodiaquine clearance and its metabolism to N-desethylamodiaquine is mediated by CYP2C8: A new high affinity and turnover enzyme-specific probe substrate, *J. Pharmacol. Exp. Ther. 300*, 399−407.
40. Attar, M., Dong, D., Ling, K. H., and Tang-Liu, D. D. (2003) Cytochrome P450 2C8 and flavin-containing monooxygenases are involved in the metabolism of tazarotenic acid in humans, *Drug Metab. Dispos. 31*, 476−481.
41. Leo, M. A., Lasker, J. M., Raucy, J. L., Kim, C. I., Black, M., and Lieber, C. S. (1989) Metabolism of retinol and retinoic acid by human liver cytochrome P4502C8, *Arch. Biochem. Biophys. 269*, 305−312.
42. Nadin, L., and Murray, M. (1999) Participation of CYP2C8 in retinoic acid 4-hydroxylation in human hepatic microsomes, *Biochem. Pharmacol. 58*, 1201−1208.
43. Rifkind, A. B., Lee, C., Chang, T. K., and Waxman, D. J. (1995) Arachidonic acid metabolism by human cytochrome P450s 2C8, 2C9, 2E1, and 1A2: Regioselective oxygenation and evidence for a role for CYP2C enzymes in arachidonic acid epoxygenation in human liver microsomes, *Arch. Biochem. Biophys. 320*, 380−389.
44. Daikh, B. E., Lasker, J. M., Raucy, J. L., and Koop, D. R. (1994) Regio- and stereoselective epoxidation of arachidonic acid by human cytochromes P450 2C8 and 2C9, *J. Pharmacol. Exp. Ther. 271*, 1427−1433.
45. Zeldin, D. C. (2001) Epoxygenase pathways of arachidonic acid metabolism, *J. Biol. Chem. 276*, 36059−36062.
46. Fisslthaler, B., Popp, R., Kiss, L., Potente, M., Harder, D. R., Fleming, I., and Busse, R. (1999) Cytochrome P450 2C is an EDHF synthase in coronary arteries, *Nature 401*, 493−497.
47. Fleming, I. (2000) Cytochrome P450 2C is an EDHF synthase in coronary arteries, *Trends Cardiovasc. Med. 10*, 166−170.
48. Fleming, I. (2001) Cytochrome P450 and vascular homeostasis, *Circ. Res. 89*, 753−762.
49. Lewis, D. F. (2002) Homology modelling of human CYP2 family enzymes based on the CYP2C5 crystal structure, *Xenobiotica 32*, 305−323.
50. Williams, P. A., Cosme, J., Sridhar, V., Johnson, E. F., and McRee, D. E. (2000) The cristallographic structure of a mammalian microsomal cytochrome P450 monooxygenase: Structural adaptations for membrane binding and functional diversity, *Mol. Cell 5*, 121.
51. Schoch, G. A., Yano, J. K., Wester, M. R., Griffin, K. J., Stout, C. D., and Johnson, E. F. (2004) Structure of human microsomal cytochrome P450 2C8. Evidence for a peripheral fatty acid binding site, *J. Biol. Chem. 279*, 9497−9503.
52. Thomas, B. J., and Rothsthein, R. (1989) Elevated recombinaison rates in transcriptionally active DNA, *Cell 56*, 619−630.
53. Truan, G., Cullin, C., Reisdorf, P., Urban, P., and Pompon, D. (1993) Enhanced in vivo monooxygenase activities of mammalian P450s in engineered yeast cells producing high levels of NADPH−P450 reductase and human cytochrome b_5, *Gene 125*, 49−55.
54. Urban, P., Cullin, C., and Pompon, D. (1990) Maximizing the expression of mammalian cytochrome-P-450 monooxygenase activities in yeast cells, *Biochimie 72*, 463−472.
55. Marques-Soares, C., Dijols, S., Macherey, A. C., Wester, M. R., Johnson, E. F., Dansette, P. M., and Mansuy, D. (2003) Sulfaphenazole derivatives as tools for comparing cytochrome P450 2C5 and human cytochromes P450 2Cs: Identification of a new high affinity substrate common to those enzymes, *Biochemistry 42*, 6363−6369.
56. Ma, Y. H., Gebremedhin, D., Schwartzman, M. L., Falck, J. R., Clark, J. E., Masters, B. S., Harder, D. R., and Roman, R. J. (1993) 20-Hydroxyeicosatetraenoic acid is an endogenous vasoconstrictor of canine renal arcuate arteries, *Circ. Res. 72*, 126−136.
57. Pompon, D., and Nicolas, A. (1989) Protein engineering by cDNA recombination in yeasts: Shuffling of mammalian cytochrome P-450 functions, *Gene 83*, 15−24.
58. Gietz, D., St. Jean, A., Woods, R. A., and Schiestl, R. H. (1992) Improved method for high efficiency transformation of intact yeast cells, *Nucleic Acids Res. 20*, 1425.
59. Bellamine, A., Gautier, J. C., Urban, P., and Pompon, D. (1994) Chimeras of the human cytochrome P450 1A family produced in yeast. Accumulation in microsomal membranes, enzyme kinetics and stability, *Eur. J. Biochem. 225*, 1005−1013.
60. Omura, T., and Sato, R. (1964) The carbon monoxide-binding pigment of liver microsomes, *J. Biol. Chem. 239*, 2370−2385.
61. Vermilion, J. L., and Coon, M. J. (1974) Highly purified detergent-solubilized NADPH-cytochrome P-450 reductase from phenobarbital-induced rat liver microsomes, *Biochem. Biophys. Res. Commun. 60*, 1315−1322.
62. Bradford, M. M. (1976) A rapid and sensitive method for the quantitation of microgram quantities of protein utilizing the principle of protein-dye binding, *Anal. Biochem. 72*, 248−254.
63. Laemmli, U. K. (1970) Cleavage of structural proteins during the assembly of the head of bacteriophage T4, *Nature 227*, 680−685.
64. Renaud, J. P., Cullin, C., Pompon, D., Beaune, P., and Mansuy, D. (1990) Expression of human liver cytochrome-P450 3A4 in yeast: A functional model for the hepatic enzyme, *Eur. J. Biochem. 194*, 889−896.
65. Spatzenegger, M., Wang, Q., He, Y. Q., Wester, M. R., Johnson, E. F., and Halpert, J. R. (2001) Amino acid residues critical for differential inhibition of CYP2B4, CYP2B5, and CYP2B1 by phenylimidazoles, *Mol. Pharmacol. 59*, 475−484.
66. Morris, G. M., Goodsell, D. S., Halliday, R. S., Huey, R., Hart, W. E., Belew, R. K., and Olson, A. J. (1998) Automated docking using a Lamarckian genetic algorithm and an empirical binding free energy function, *J. Comput. Chem. 19*, 1639−1662.
67. Helms, V., and Wade, R. C. (1995) Thermodynamics of water mediating protein−ligand interactions in cytochrome P450cam: A molecular dynamics study, *Biophys. J. 69*, 810−824.
68. van Aalten, D. M., Bywater, R., Findlay, J. B., Hendlich, M., Hooft, R. W., and Vriend, G. (1996) PRODRG, a program for generating molecular topologies and unique molecular descriptors from coordinates of small molecules, *J. Comput.-Aided Mol. Des. 10*, 255−262.
69. McSorley, L. C., and Daly, A. K. (2000) Identification of human cytochrome P450 isoforms that contribute to all-trans-retinoic acid 4-hydroxylation, *Biochem. Pharmacol. 60*, 517−526.
70. Busse, D., Cosme, J., Beaune, P., Kroemer, H. K., and Eichelbaum, M. (1995) Cytochromes of the P450 2C subfamily are the major enzymes involved in the O-demethylation of verapamil in humans, *Naunyn-Schmiedeberg's Arch. Pharmacol. 353*, 116−121.
71. Tracy, T. S., Korzekwa, K. R., Gonzalez, F. J., and Wainer, I. W. (1999) Cytochrome P450 isoforms involved in metabolism of the enantiomers of verapamil and norverapamil, *Br. J. Clin. Pharmacol. 47*, 545−552.
72. Wester, M. R., Johnson, E. F., Marques-Soares, C., Dansette, P. M., Mansuy, D., and Stout, C. D. (2003) Structure of a substrate complex of mammalian cytochrome P450 2C5 at 2.3 Å Resolu-

tion: Evidence for multiple substrate binding modes, *Biochemistry 42*, 6370−6379.
73. Wester, M. R., Johnson, E. F., Marques-Soares, C., Dijols, S., Dansette, P. M., Mansuy, D., and Stout, C. D. (2003) Structure of mammalian cytochrome P450 2C5 complexed with diclofenac at 2.1 Å resolution: Evidence for an induced fit model of substrate binding, *Biochemistry 42*, 9335−9345.
74. Gotoh, O. (1992) Substrate recognition sites in cytochrome P450 family 2 (CYP2) proteins inferred from comparative analyses of amino acid and coding nucleotide sequences, *J. Biol. Chem. 267*, 83−90.
75. Mancy, A., Antignac, M., Minoletti, C., Dijols, S., Mouries, V., Duong, N. T., Battioni, P., Dansette, P. M., and Mansuy, D. (1999) Diclofenac and its derivatives as tools for studying human cytochromes P450 active sites: Particular efficiency and regioselectivity of P450 2Cs, *Biochemistry 38*, 14264−14270.
76. Kleywegt, G. J., and Jones, T. A. (1994) Detection, delineation, measurement and display of cavities in macromolecular structures, *Acta Crystallogr. D50*, 178−185.
77. Kerdpin, O., Elliot, D. J., Boye, S. L., Birkett, D. J., Yoovathavorm, K., and Miners, J. O. (2004) Differential contribution of active site residues in substrate recognition sites 1 and 5 to cytochrome P450 2C8 substrate selectivity and regioselectivity, *Biochemistry 43*, 7834−7842.

BI0489309